

# Determining Shape and Reflectance of Hybrid Surfaces by Photometric Sampling

SHREE K. NAYAR, MEMBER, IEEE, KATSUSHI IKEUCHI, MEMBER, IEEE, AND TAKEO KANADE, SENIOR MEMBER, IEEE

**Abstract**—Machine vision can benefit greatly from the development and utilization of accurate reflectance models. Our hybrid reflectance model is a linear combination of Lambertian and specular components and is obtained from the primary reflection components by making surface assumptions. Hence, Lambertian and specular surfaces are special instances of hybrid surfaces. We present a method for determining the shapes of hybrid surfaces without prior knowledge of the relative strengths of the Lambertian and specular components of reflection. The object surface is illuminated using extended light sources and is viewed from a single direction. Surface illumination using extended sources makes it possible to ensure the detection of both Lambertian and specular reflections. Uniformly distributed source directions are used to obtain an image sequence of the object. This method of obtaining photometric measurements is called photometric sampling. An extraction algorithm uses the set of image intensity values measured at each surface point to compute orientation as well as relative strengths of the Lambertian and specular reflection components. The simultaneous recovery of shape and reflectance parameters enables the method to adapt to variations in reflectance properties from one scene point to another. Experiments were conducted on Lambertian surfaces, specular surfaces, and hybrid surfaces. The measured surface orientations are found to be highly accurate, and the estimated reflectance parameters are consistent with the reflectance characteristics of the surfaces.

## I. INTRODUCTION

**M**OST MACHINE vision problems involve the analysis of images resulting from the reflection of light. The apparent brightness of a point depends on its ability to reflect incident light in the direction of the sensor; this is commonly known as its reflectance properties. Therefore, the prediction or interpretation of image intensities requires a sound understanding of the various mechanisms involved in the reflection process. Although shape extraction methods are being developed and refined, it is also essential for the vision community to research and utilize more sophisticated reflectance models. Once a "general" reflectance model is made available, we are free to make reflectance assumptions that are appropriate for the vision application at hand. The result, a more specific model, may then be used to develop efficient shape extraction techniques.

Shape from shading [4], [6], [13], photometric stereo [2], [7], [18], and local shape from specularity [3] are examples

of techniques that extract three-dimensional shape information from image intensities. All of these techniques rely on prior knowledge of surface reflectance properties. The reflectance properties are either assumed or measured using a calibration object of known shape. In many real-world applications, such as those involving surfaces of different reflectance characteristics, the calibration approach is not a practical one. Therefore, existing shape extraction methods are often used by assuming surface reflectance to be either Lambertian or specular. Many surfaces encountered in practice are hybrid in reflectance, that is, their reflectance models are linear combinations of Lambertian and specular models. Therefore, Lambertian and specular models are only limiting instances of the hybrid model. It is desirable to have a method that is capable of extracting the shape of hybrid surfaces including, as special cases, those that are purely Lambertian or specular.

In many industrial applications, surface polish and roughness are found to be important inspection criteria. In such cases, surface reflectance properties may be interpreted as measures of these criteria. Furthermore, reflectance properties may be used to segment an image into different regions; each region may then be regarded as a different surface to aid the process of inspection. For these reasons, it would be of great value to have a technique that could, in addition to determining shape, also estimate the reflectance properties of each surface point.

We begin this paper with a summary of the various mechanisms involved in the reflection process. By considering both physical optics and geometrical optics approaches, the primary components of reflection are identified. By making assumptions related to the microscopic shape of surfaces, the primary reflection components are simplified to obtain the hybrid reflectance model. The object of interest is illuminated using multiple extended light sources and is viewed from a single direction. The sources are uniformly distributed around the object and are sequentially scanned, one by one, to obtain an image sequence of the object. We refer to this method of obtaining photometric measurements as *photometric sampling*. An extraction algorithm uses the image sequence and the hybrid reflectance model to determine object shape. Shape information is extracted *without* prior knowledge of the relative strengths of the Lambertian and specular reflection components. In addition, the extraction algorithm also estimates reflectance parameters at surface points. The *simultaneous* recovery of shape and reflectance enables the method to adapt to variations in hybrid reflectance from one surface point to the next.

Manuscript received November 1, 1988; revised March 14, 1990. This work was supported by Westinghouse Electric Corporation and by DARPA under Contract F33615-87-C-1499.

S. K. Nayar is with the Department of Electrical and Computer Engineering and the Robotics Institute, Carnegie Mellon University, Pittsburgh, PA 15213.

K. Ikeuchi and T. Kanade are with the Department of Computer Science and the Robotics Institute, Carnegie Mellon University, Pittsburgh, PA 15213.  
IEEE Log Number 9037734.

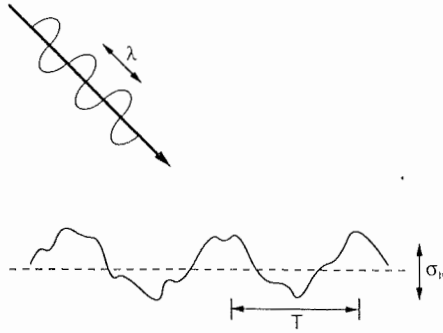


Fig. 1. Surface reflection is closely related to the microscopic surface profile and the wavelength of incident light.

## II. SURFACE REFLECTION

### A. A Unified Perspective

When light is incident on a boundary interface between two different media, it is reflected according to well-known laws. There are two different approaches to optics and, consequently, two different approaches to the study of reflection. Physical or wave optics is based directly on electromagnetic wave theory and uses Maxwell's equations to study the propagation of light. Geometrical or ray optics on the other hand, uses the short wavelength of light to simplify many of the light propagation problems. Although geometrical reflectance models may be construed as mere approximations to physical reflectance models, they possess simpler mathematical forms that often render them more usable than physical models. However, geometrical models are applicable only when the wavelength of incident light is small when compared to the dimensions of the *microscopic* surface imperfections. Therefore, it is incorrect to use these models to interpret or predict reflections from smooth surfaces; only physical models are capable of describing the underlying reflection mechanism.

In [11], we have unified physical and geometrical approaches to describe reflection from surfaces that may vary from smooth to rough. More specifically, we have focused on the Beckmann–Spizzichino (physical optics) model and the Torrance–Sparrow (geometrical optics) model. The surface height is modeled as a continuous stationary random process with standard deviation  $\sigma_h$  representing the physical *roughness* of the surface (Fig. 1). The spatial variation of the surface is described in terms of a correlation function that represents the dependence between the heights of different points on the surface. The spatial frequency of the surface is determined by the correlation distance  $T$ . The incident light is assumed to be a plane electromagnetic wave with wavelength  $\lambda$ . The reflectance curves predicted by the physical and geometrical models are obtained by varying the three parameters  $\sigma_h$ ,  $T$ , and  $\lambda$ . From studying the behaviors of the physical and geometrical optics models, it is seen that surface radiance may be decomposed into three primary reflection components, namely, the *diffuse lobe*, the *specular lobe*, and the *specular spike*.

The diffuse component results from two main mechanisms. In one case, light rays that impinge on the surface are reflected many times between surface undulations before they are scattered into space. If these *multiple reflections* occur

in a random manner, the incident energy is distributed in all directions, resulting in diffuse reflection. Another mechanism leading to diffuse reflection is the *internal scattering*<sup>1</sup> of light rays. In this case, the light rays penetrate the surface and encounter microscopic inhomogeneities in the surface medium. The light rays are repeatedly reflected and refracted at boundaries between regions of differing refractive indices. Some of the scattered rays find their way back to the surface in a variety of directions, resulting in diffuse reflection.

Specular reflection is composed of two primary components: the specular lobe and the specular spike. The lobe component spreads around the specular direction, and the spike component is zero in all directions except for a very narrow range around the specular direction. The relative strengths of the two components are dependent on the microscopic roughness of the surface. A detailed analysis of the characteristics of the three reflection components is given in [11]. We summarize our findings with the following remarks:

- The diffuse component may be represented by the Lambertian model [9]. This model has been used extensively to test shape-from-shading and photometric stereo techniques, and the results have indicated that it performs reasonably well. More accurate models [8], [14] may be used at the cost of functional complexity.
- The Beckmann–Spizzichino physical optics model predicts both the specular lobe and spike components. For a very smooth surface ( $\sigma_h \ll \lambda$ ), the spike component dominates, and the surface behaves like a mirror. As the roughness increases, however, the spike component shrinks rapidly, and the lobe component begins to dominate. The two components are simultaneously significant for only a small range of roughness values.
- A “sharp” specular component may result from the specular spike component when the surface is smooth ( $\sigma_h/\lambda < 1.5$ ) and/or the specular lobe component when the surface is gently undulating ( $\sigma_h/T < 0.02$ ).
- The Torrance–Sparrow geometrical optics model provides a good approximation of the specular lobe component of the Beckmann–Spizzichino model. Both models are successful in predicting *off-specular* peaks in the specular lobe component. Due to its simpler mathematical form, the Torrance–Sparrow model may be used to represent the specular lobe component.
- The Torrance–Sparrow model is not capable of describing the mirror-like behavior of smooth surfaces, and it should not be used to represent the specular spike component because it would produce erroneous results.
- The specular lobes of both Torrance–Sparrow and Beckmann–Spizzichino models tend to have *specular peaks*, rather than off-specular peaks, when the viewing direction is fixed and the source direction is varied.

In shape extraction techniques such as photometric stereo and structured highlight, images of the observed object are obtained by varying the source direction while keeping the viewing direction constant. The shape extraction method de-

<sup>1</sup> This mechanism is often referred to as “body” reflection.

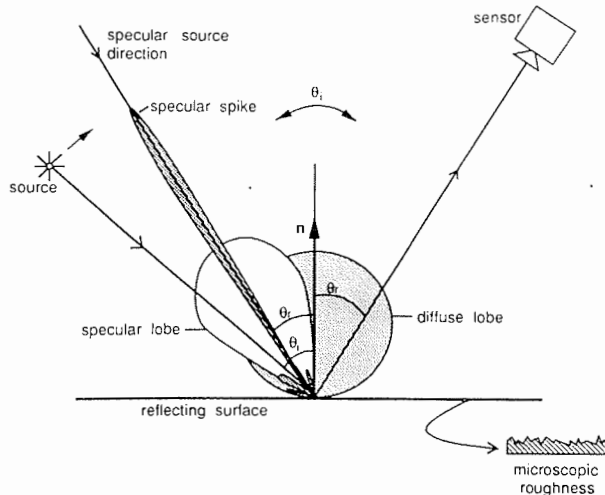


Fig. 2. Polar plots of the primary reflection components as functions of the source angle for a given viewing direction.

scribed in this paper is based on the same approach. The shapes and functional forms of individual reflection components are different for the case in which the viewing direction is varied and the case in which the source direction is varied. We emphasize this difference by introducing a new representation of the reflection components. Fig. 2 shows polar plots of the diffuse lobe, specular lobe, and specular spike. The magnitudes of the three components of surface radiance in the sensor direction are determined by intersections made by the lobes with the line joining the source and the origin. The diffuse component is represented by the Lambertian model, the specular lobe component by the Torrance-Sparrow model, and the specular spike component by the spike component of the Beckmann-Spizzichino model.

### B. Hybrid Reflectance Model

In this paper, we assume that the surfaces of interest are smooth, i.e., either the surface roughness is comparable to the wavelength of incident light ( $\sigma_h/\lambda < 1.5$ ), or the surface is gently undulating ( $\sigma_h/T < 0.02$ ), or both. From the previous discussion we see that under these conditions, both the spike and lobe components can be significant only in a narrow region around the specular direction. Therefore, we will combine the spike and lobe components into a single component, namely, the *specular component*. We also assume that the surfaces under consideration are nonhomogeneous. Therefore, a diffuse component of reflection may result from the internal scattering mechanism. We use the Lambertian model to represent the diffuse component. The combination of the above-mentioned two components is referred to as the *hybrid reflectance model*.

Consider the illumination of an object by a point source of light, as is shown in Fig. 3. Light energy reflected by the surface in the direction of the camera causes an image of the surface to be formed. The intensity at any point in the image of the surface may be expressed as

$$I = IL + IS \quad (1)$$

where  $IL$  is the Lambertian intensity component, and  $IS$  is the specular intensity component.

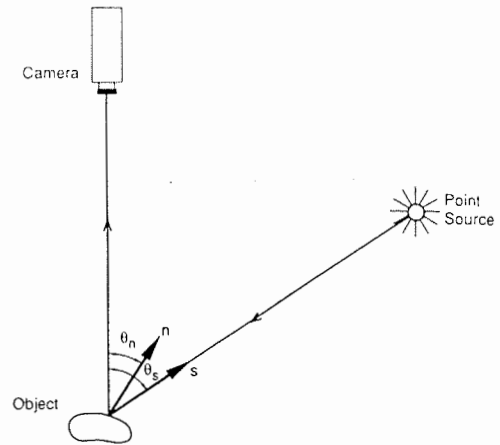


Fig. 3. Two-dimensional illumination and imaging geometry. A surface element with orientation  $\theta_n$  reflects light from the point source direction  $\theta_s$  into the camera.

We will express the two components of image intensity in terms of the parameters that describe the two-dimensional imaging and illumination geometry shown in Fig. 3. In two dimensions, the source direction vector  $s$ , surface normal vector  $n$ , and viewing direction vector  $v$  lie in the same plane. Therefore, directions are represented by a single parameter, namely, the zenith angle  $\theta$ .

1) *Lambertian Component*: The brightness of a Lambertian surface is proportional to the energy of incident light. As can be seen in Fig. 3, the amount of light energy falling on a surface element is proportional to the area of the surface element as seen from the source position, which is often referred to as the foreshortened area. The foreshortened area is a cosine function of the angle between the surface orientation direction  $\theta_n$  and the source direction  $\theta_s$ . Therefore, the Lambertian intensity component  $IL$  may be written as

$$IL = A \cos(\theta_s - \theta_n) \quad (2)$$

where the constant  $A$  determines the fraction of incident energy that is diffusely reflected. We have assumed that the angle of incidence ( $\theta_s - \theta_n$ ) is greater than  $-\pi/2$  and less than  $\pi/2$ , i.e.,  $IL$  is always greater than zero.

2) *Specular Component*: Since the specular intensity component  $IS$  is a very sharp function of the source direction, it may be approximated by the delta function [11]

$$IS = B\delta(\theta_s - 2\theta_n). \quad (3)$$

The basic *photometric function*<sup>2</sup> relates image intensity to surface orientation, surface reflectance, and point source direction and may be written by substituting (2) and (3) into (1) to obtain

$$I = A \cos(\theta_s - \theta_n) + B\delta(\theta_s - 2\theta_n). \quad (4)$$

The constants  $A$  and  $B$  in (4) represent the relative strengths of the Lambertian and specular components of reflection, respectively. We call  $A$  and  $B$  the reflectance parameters. We

<sup>2</sup> The photometric function is similar to the image irradiance [5] equation since image intensity is assumed to be proportional to image irradiance.

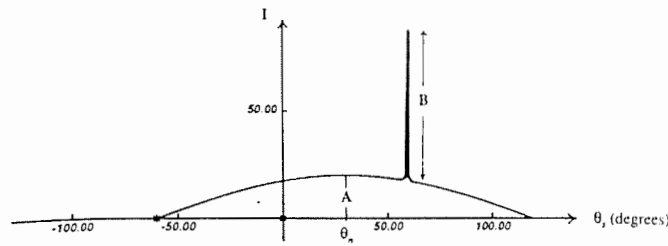


Fig. 4. Basic photometric function  $I(\theta_s)$  for a hybrid surface.

see that  $A > 0$  and  $B = 0$  for a purely Lambertian surface,  $A = 0$  and  $B > 0$  for a purely specular surface, and  $A > 0$  and  $B > 0$  in general.

Our objective is to determine orientation and reflectance at each surface point from a set of image intensities that result from changing the source direction  $\theta_s$ . Therefore, we will often refer to the basic photometric function as  $I(\theta_s)$ , which is a relation between image intensity and source direction. Fig. 4 shows a plot of the basic photometric function for a hybrid surface of given orientation.

### III. PHOTOMETRIC SAMPLING USING EXTENDED SOURCES

#### A. Why Extended Sources?

We propose to illuminate the object surface by using extended sources, rather than point sources, for the following reasons:

- In the case of point source illumination, specular reflection is not detected unless  $\theta_s = 2\theta_n$  exactly. In order to determine shape and reflectance parameters of specular and hybrid surfaces, specular reflections must be captured in the measured intensities. To detect specular reflections from surface points of all orientations, an infinite number of point sources need to be positioned around the surface. Such an approach is unrealistic from the perspective of practical implementation. Unlike a point source, an extended source emits light from an area of points rather than a single point. Therefore, a small number of extended sources may be used to ensure the detection of specular reflections.
- In the case of point source illumination, image intensities due to specular reflections are often observed to be much greater than intensities resulting from Lambertian reflections [15]. Therefore, it is difficult to measure both components in the same image. Extended source illumination tends to make the image intensities due to Lambertian and specular reflections comparable to one another. A specular surface element of a given orientation will reflect light from a small area on the extended source into the camera. On the other hand, a Lambertian surface element of the same orientation reflects light from all points on the extended source into the camera. This feature of the proposed illumination scheme makes it possible to measure both Lambertian and specular reflections in the same image.

In Appendix A, we have shown how extended sources are generated. The extended source radiance function  $L(\theta, \theta_s)$  is derived, and the parameters that determine the direction and

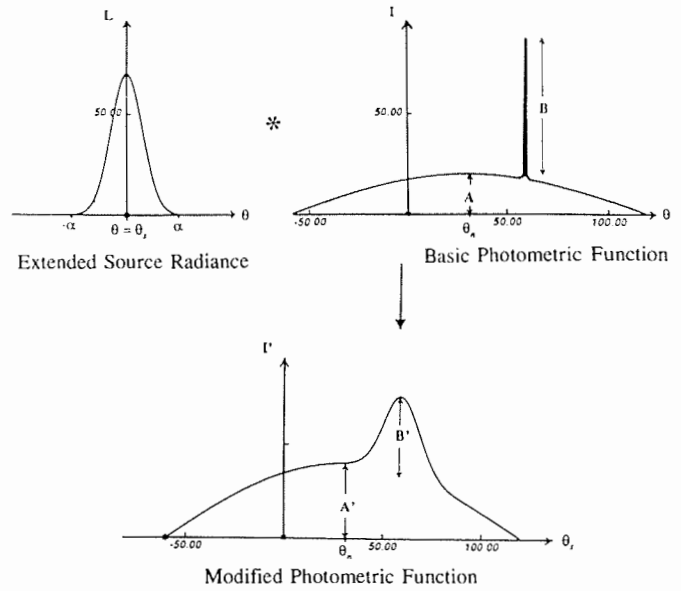


Fig. 5. Photometric function for extended source illumination is obtained by convolving the basic photometric function with the extended source radiance function.

limits of an extended source are defined. These results will be extensively used in the following discussions.

#### B. Photometric Function for Extended Sources

The photometric function for point source illumination (see (4)) needs to be modified for extended source illumination. An extended source may be thought of as a collection of point sources in which each point source has a radiant intensity that is dependent on its position on the extended source. The intensity of light reflected by a surface may be determined by computing the integral of the light energies reflected from all points on the extended source. Therefore, the modified photometric function  $I'(\theta_s)$  is determined by convolving the basic photometric function  $I(\theta)$  with the extended source radiance function  $L(\theta, \theta_s)$ . This operation is illustrated in Fig. 5. For a surface point of orientation  $\theta_n$ , the Lambertian component  $IL'$  of the modified photometric function is determined to be

$$IL' = A \int_{\theta_s - \alpha}^{\theta_s + \alpha} L(\theta, \theta_s) \cos(\theta - \theta_n) d\theta. \quad (5)$$

The limits of the integral are determined by the width of the extended source (Appendix A). It can be shown [10] that  $IL'$  is a cosine function of the angle between the surface orientation and the direction corresponding to the "center of mass" of the extended source radiance distribution  $L(\theta, \theta_s)$ . In our case, since the extended source is symmetric with respect to the source direction  $\theta_s$ , the center of mass of the radiance function is in the direction  $\theta_s$ . Therefore, we obtain

$$IL' = A' \cos(\theta_s - \theta_n) \quad (6)$$

where the constant  $A'$  is proportional to  $A$  [10] and, hence, also represents the strength of the Lambertian component.

Similarly, the specular intensity component  $IS'$  resulting

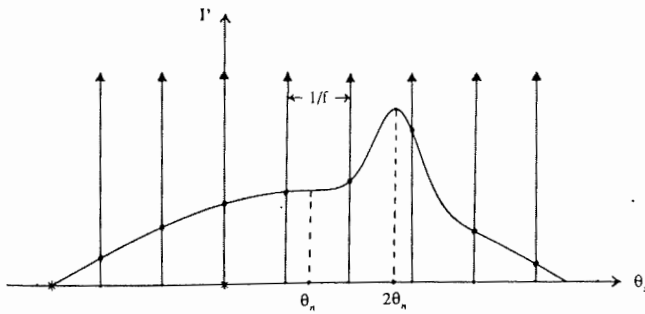


Fig. 6. Sampling the modified photometric function.

from the extended source  $L(\theta, \theta_s)$  is determined to be

$$IS' = B \int_{\theta_s - \alpha}^{\theta_s + \alpha} L(\theta, \theta_s) \delta(\theta - 2\theta_n) d\theta \quad (7)$$

or

$$IS' = BL(2\theta_n, \theta_s). \quad (8)$$

Strictly speaking, the result of the above integral is dependent on the exact shape of the specular spike and lobe. However, since both components are significant only in the specular direction  $2\theta_n$ , it is reasonable to assume that the specular intensity  $IS'$  is proportional to  $L(2\theta_n, \theta_s)$ , whereas the constant of proportionality is dependent on the exact shape of the two components. In light of this, we will use the constant  $B'$ , rather than  $B$ , to represent the strength of the specular component of the photometric function.

The *modified photometric function* relates image intensity  $I'$  to extended source direction  $\theta_s$  and is expressed as the sum of the components  $IL'$  and  $IS'$ :

$$I' = A' \cos(\theta_s - \theta_n) + B'L(2\theta_n, \theta_s). \quad (9)$$

Since the parameters  $A'$  and  $B'$  are proportional to the parameters  $A$  and  $B$ , respectively, they may be used to represent the reflectance properties of the surface point.

### C. Sampling

The process of measuring image intensities corresponding to different source directions is equivalent to sampling the modified photometric function  $I'(\theta_s)$ , as is shown in Fig. 6. Samples of the photometric function may be obtained by moving an extended source around the object and obtaining images of the object for different source positions. An alternative approach would be to distribute an array of extended sources around the object such that each source illuminates the object from a different direction. The entire array of extended sources may be sequentially scanned such that for each scan, a single source is active, and an image of the object surface is obtained. We have chosen to use this alternative approach in our experiments. We will confine the sampling process to two dimensions: the surface normal vector, viewing direction vector, and source direction vectors for all extended sources, are coplanar. The sequential scanning of extended sources positioned in the directions  $\{\theta_i: i = 1, 2, \dots, M\}$  results in a set of image intensities  $\{I'_i: i = 1, 2, \dots, M\}$  measured at each point on the object surface.

The number of samples measured at each surface point is determined by the frequency  $f$  at which  $I'(\theta_s)$  is sampled. In order to extract the shape and the reflectance parameters of hybrid surfaces, both Lambertian and specular components of image intensity must be detected. Since we have used a delta function for the specular reflection model, the period of the modified photometric function that contains specular intensities is equal to the width  $2\alpha$  of the extended source radiance function. In the following section, we will show that in general, at least two photometric samples must have nonzero specular intensities for the extraction technique to work. Hence, the photometric function must be sampled at a frequency greater than or equal to the *minimum sampling frequency*<sup>3</sup>  $f_{\min}$ , where

$$f_{\min} = \frac{1}{\alpha}. \quad (10)$$

Note that at this minimum frequency, the radiance distributions of adjacent extended sources overlap each other for an interval of  $\alpha$ .

## IV. EXTRACTING SHAPE AND REFLECTANCE

Given the set of image intensities  $\{I'_i\}$  measured at a surface point, we want to determine the orientation  $\theta_n$  and reflectance parameters  $A'$  and  $B'$  of the point. We will first develop techniques to compute orientations of purely Lambertian and purely specular surfaces. Later, these techniques will be used to extract orientations and reflectance parameters of *general hybrid surfaces*.

### A. Lambertian Surfaces

Consider the case where the surface of an object is known to be purely Lambertian. The task is to determine the shape of the object. The photometric samples for a Lambertian surface point may be written as

$$I'_i = A' \cos(\theta_i - \theta_n). \quad (11)$$

We would like to compute the orientation  $\theta_n$  and the strength of the Lambertian reflection component  $A'$ .

Toward this end, an error  $E$  is formulated to be the sum of the errors in measured samples over the entire set of samples:

$$E = \sum_{i=1}^M [I'_i - A' \cos(\theta_i - \theta_n)]^2. \quad (12)$$

By using the conditions

$$\frac{\partial E}{\partial \theta_n} = 0 \quad \text{and} \quad \frac{\partial E}{\partial A'} = 0 \quad (13)$$

we can determine values of  $\theta_n$  and  $A'$  that minimize the error  $E$ . The above minimization is simplified by expressing  $\cos(\theta_i - \theta_n)$  as a dot product of the source and normal vectors.

<sup>3</sup> It is assumed that the interval of the modified photometric function that contains specular intensities is small compared with the total width of the photometric function. Therefore, sampling frequencies that ensure the detection of specular intensities will provide a sufficient number of Lambertian intensity samples.

*B. Specular Surfaces*

Now consider the case where the object surface is known to be purely specular, and the shape of the object is to be determined. The photometric samples for a specular point may be written as

$$I'_i = B' L(2\theta_n, \theta_i). \quad (14)$$

We wish to determine the orientation  $\theta_n$  and the specular strength  $B'$  from the intensity set  $\{I'_i\}$ . Let us assume that the specular direction  $2\theta_n$  lies between the directions  $\theta_k$  and  $\theta_{k+1}$  of two adjacent extended sources. Further, let us assume that the photometric function is sampled using the minimum frequency  $f_{\min}$ , i.e.,  $\theta_{k+1} = \theta_k + \alpha$ . Then, since the surface is specular, only the samples  $I'_k$  and  $I'_{k+1}$  will have nonzero values. We see that when  $\theta_n$  increases,  $2\theta_n$  approaches  $\theta_{k+1}$ ,  $I'_k$  decreases, and  $I'_{k+1}$  increases. Similarly, when  $\theta_n$  decreases,  $2\theta_n$  approaches  $\theta_k$ ,  $I'_k$  increases, and  $I'_{k+1}$  decreases. In fact, from (14), we see that the intensity ratio  $I'_k/I'_{k+1}$  is equal to the ratio  $L(2\theta_n, \theta_k)/L(2\theta_n, \theta_{k+1})$ . Since the extended sources have decaying radiance functions (Appendix A), this ratio is a monotonic function of the angle  $2\theta_n$ . Since the radiance functions of the extended sources are known *a priori*, we can precompute and store in memory the correspondence between  $I'_k/I'_{k+1}$  and  $\theta_n$ .

Given the image intensity set  $\{I'_i\}$  at a specular surface point, the nonzero image intensities in the set are first identified. If only a single intensity value, for instance  $I'_k$ , is greater than zero, then we know that  $2\theta_n = \theta_k$ . If two image intensities, say  $I'_k$  and  $I'_{k+1}$ , are greater than zero, the ratio  $I'_k/I'_{k+1}$  is used to determine  $\theta_n$ . Once  $\theta_n$  is found,  $B'$  is obtained by using (14):

$$B' = \frac{I'_k}{L(2\theta_n, \theta_k)}. \quad (15)$$

*C. Hybrid Surfaces*

The modified photometric function for hybrid surfaces is given by (9). At each surface point, we want to determine  $A'$ ,  $B'$ , and orientation  $\theta_n$  from the measured samples  $\{I'_i: i = 1, 2, \dots, M\}$  of the photometric function. Toward this end, we will develop an algorithm that attempts to separate the Lambertian and specular components of each measured image intensity and then computes surface orientations using the methods given above for Lambertian and specular surfaces.

The extraction algorithm is based on two constraints, namely, the *sampling frequency constraint* and the *unique orientation constraint*. By sampling the modified photometric function at the minimum sampling frequency  $f_{\min}$ , we can ensure that only two consecutive image intensities in the intensity set  $\{I'_i\}$  contain nonzero specular components. For each  $k$  in the interval  $0 < k < M$ ,  $I'_k$  and  $I'_{k+1}$  are hypothesized as being the two intensities that have specular components. All remaining intensities in the set  $\{I'_i: i = 1, 2, \dots, M\}$  must represent only Lambertian components of reflection. These intensities are used to compute the surface orientation  $\theta_{nl}$  and the Lambertian strength  $A'$  (Section IV-A). The Lambertian components  $IL'_k$  and  $IL'_{k+1}$  are determined and used to sep-

arate the specular components  $IS'_k$  and  $IS'_{k+1}$  from  $I'_k$  and  $I'_{k+1}$ , respectively. The surface orientation  $\theta_{ns}$  and specular strength  $B'$  are computed from  $IS'_k$  and  $IS'_{k+1}$  (Section IV-B).

Next, the physical constraint that each surface point has a unique orientation is exploited. An estimate  $\theta_{nk}$  of the orientation is found as a weighted average of the orientations  $\theta_{nl}$  and  $\theta_{ns}$ . The weights are proportional to the strengths of the two components of reflection. We support this method of weight selection because the surface orientation that is computed from intensities resulting from the stronger of the two reflection components is less sensitive to image noise and is, therefore, more reliable. An orientation error  $e_k$  is found by comparing  $\theta_{nk}$  with  $\theta_{nl}$  and  $\theta_{ns}$ . Using the above approach, orientation errors are computed for all  $k$ , where  $0 < k < M$ . The orientation and reflectance parameters computed for the value of  $k$  that minimizes the orientation error are assigned to the surface point under consideration. This process is repeated for all points on the object surface.

It is important to note that the extraction algorithm is also capable of determining shape and reflectance of purely Lambertian and purely specular surfaces.

*1) Extraction Algorithm:*

**Step 1:** If all intensities  $I'_i$  measured at the image point  $(x, y)$  are less than the minimum intensity threshold  $T$ , assign the point  $(x, y)$  to "background" and **stop**.

**Step 2:** Let  $k = 1$  and  $e_0$  equal a large positive number.

**Step 3:** Assume that image intensities  $I'_k$  and  $I'_{k+1}$  consist of nonzero specular components of reflection. All remaining intensities  $I'_i$  (where  $i \neq k$  and  $i \neq k + 1$ ) are used with the Lambertian model to compute the surface orientation  $\theta_{nl}$  and Lambertian strength  $A'_k$  (Section IV-A).

**Step 4:** The specular components  $IS'_k$  and  $IS'_{k+1}$  are separated from the image intensities  $I'_k$  and  $I'_{k+1}$ :

$$IS'_k = I'_k - A'_k \cos(\theta_k - \theta_{nl})$$

$$IS'_{k+1} = I'_{k+1} - A'_k \cos(\theta_{k+1} - \theta_{nl}). \quad (16)$$

If  $IS'_k < 0$  or  $IS'_{k+1} < 0$ , set  $k = k + 1$  and go to **Step 2**.

**Step 5:** If  $IS'_k = 0$  and  $IS'_{k+1} = 0$ , let  $B'_k = 0$ . Otherwise, determine the surface orientation  $\theta_{ns}$  and the specular strength  $B'_k$  by using specular intensities  $IS'_k$  and  $IS'_{k+1}$  and the specular model (Section IV-B).

**Step 6:** The best estimate of surface orientation, for the  $k$ th iteration, is determined to be

$$\theta_{nk} = \frac{A'_k \theta_{nl} + B'_k \theta_{ns}}{A'_k + B'_k}. \quad (17)$$

The orientation error  $e_k$  is determined to be

$$e_k = \frac{A'_k |\theta_{nl} - \theta_{nk}| + B'_k |\theta_{ns} - \theta_{nk}|}{A'_k + B'_k}. \quad (18)$$

**Step 7:** If  $e_k < e_{k-1}$ , then

$$\theta_n = \theta_{nk}, \quad A' = A'_k, \quad B' = B'_k. \quad (19)$$

If  $k < M - 1$ , set  $k = k + 1$  and go to **Step 2**. Otherwise, **stop**.

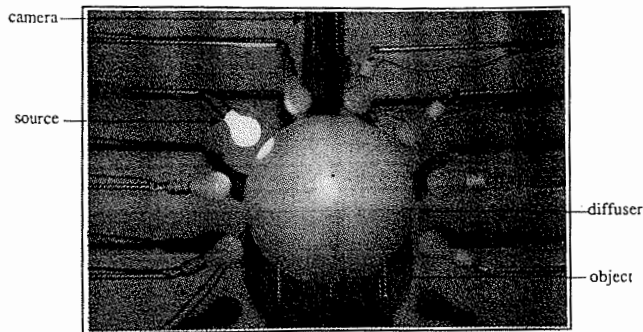


Fig. 7. Photograph of the experimental setup used to demonstrate the photometric sampling concept.

In order to account for errors in image intensities due to the presence of noise, the implemented version of the above algorithm uses upper and lower bounds while testing inequalities, such as  $IS'_k < 0$  and  $IS'_{k+1} < 0$ .

## V. EXPERIMENTS

### A. Experimental Setup

We have conducted experiments to demonstrate the practical feasibility of the photometric sampling concept. A photograph of the experimental setup used to implement photometric sampling is shown in Fig. 7. A 14-in diameter lamp shade is used as the spherical diffuser, and extended light sources are generated on the diffuser's surface by illuminating it using incandescent light bulbs. All light bulbs are assumed to have the same radiant intensity and are equidistant from the center of the diffuser. In our experiments, a source termination angle of  $\alpha = 32^\circ$  is used, and sampling is performed at the minimum frequency determined by (10). The object is placed at the center of the diffuser and is viewed by a camera through a 1-in diameter hole at the top of the diffuser. The current setup uses a WV-22 model Panasonic CCD camera that has a  $512 \times 480$  pixel resolution. The complete imaging system, which is comprised of lenses and camera, has a physical resolution of 0.002 in per pixel width. In the current implementation, the light bulbs, camera, and object are all placed in the same plane. This two-dimensional setup is capable of measuring only orientations of surface normal vectors that lie on a single plane in orientation space. For each extended source, an image of the object is digitized and stored in memory. The sequence of object images, which are generated by scanning the array of extended sources, is processed on a 3/60 SUN workstation.

### B. Results

Fig. 8 shows photometric samples measured at a point on the surface of a plastic object using the above experimental setup. The measured intensity values are represented by black dots. The reflectance model of the plastic surface includes both Lambertian and specular components. The orientation of the surface point was known *a priori*. Using the orientation value, the two measured samples that were expected to consist of both Lambertian and specular intensities were identified and are marked in the figure as "L+S". All remaining image intensities result from Lambertian reflection and are marked

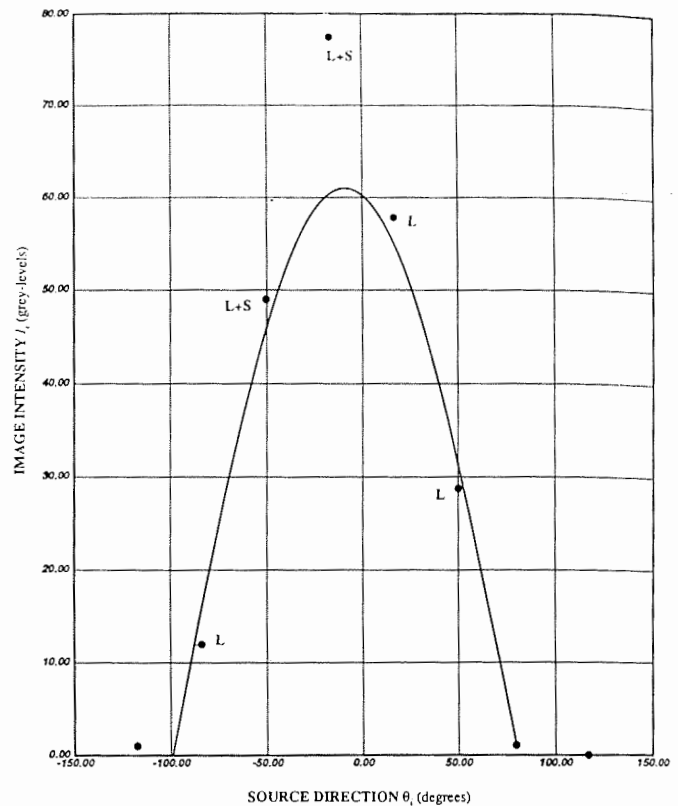
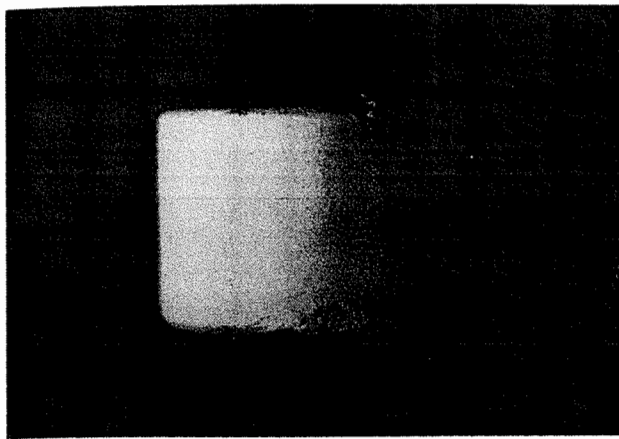


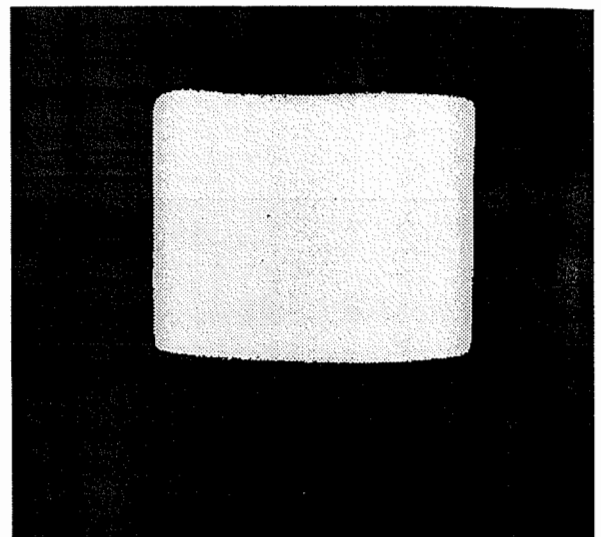
Fig. 8. Samples of the photometric function measured at a hybrid surface point. By using the known orientation of the surface point, the two intensities that have specular reflections are identified and marked "L+S." The remaining points result solely from Lambertian reflection, and the cosine function that best fits these points is shown as a solid curve.

in the figure as "L." The cosine function that best fits the Lambertian intensities is represented by the solid curve. The specular components were extracted from the two intensities that are marked as "L+S." Two estimates of surface orientation were computed using the Lambertian and the specular components of the image intensities. Both computed orientations were found to be within  $2.5^\circ$  of the actual orientation value. Similar experiments were conducted on Lambertian and specular surfaces [10]. The results indicated that the hybrid model used in this paper does quite well in describing reflectance of light by smooth surfaces.

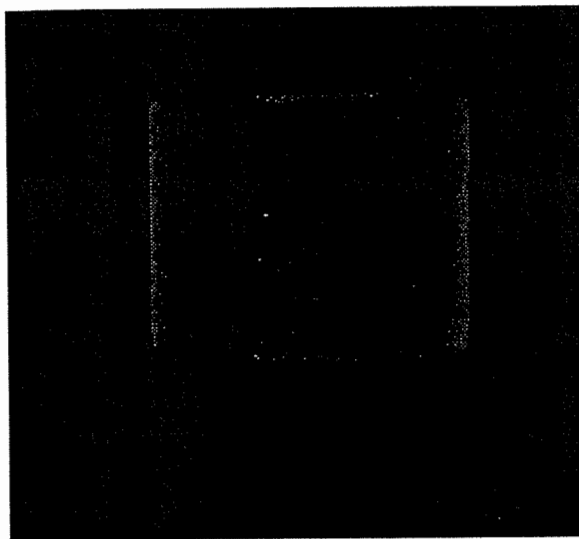
The experimental setup and the extraction algorithm were used to extract surface properties of a number of objects. Figs. 9, 10, 11, and 12 show the results of the extraction method applied to objects with different surface reflectance properties. For each object, a photograph of the object is followed by two reflectance images (Lambertian and specular), a needle map produced by the extraction algorithm, and a depth map that is constructed from the needle map. The intensity at each pixel in the reflectance images is proportional to the strength of the reflectance model component the image represents. The needle map is a representation of surface orientations. At each point on a needle map, the length of the needle is proportional to the tilt of the surface away from the viewing direction of the camera. All needles originate from the dots that constitute the resolution grid of the needle map. To help evaluate the performance of the extraction algorithm, we have included a



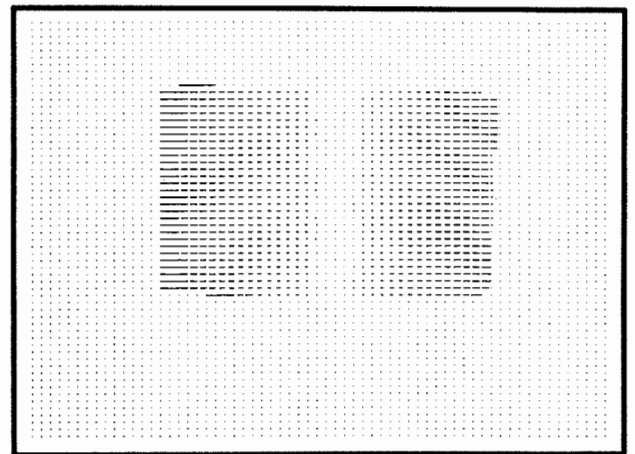
(a)



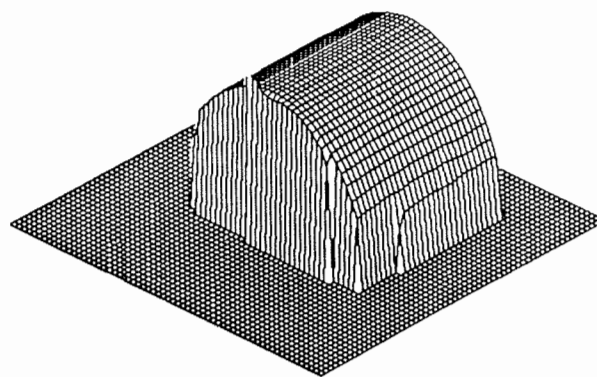
(b)



(c)



(d)



(e)

Fig. 9. Cylindrical painted object with a Lambertian surface: (a) Object; (b) Lambertian strength; (c) specular strength; (d) needle map; (e) depth map.

depth map of each object that is obtained by integrating the orientations in the needle map. Note that the reconstructed surfaces are displayed at some arbitrary offset level in all the depth maps.

The object shown in Fig. 9 is cylindrical and its surface is Lambertian. Fig. 10 is the photo of a prism-shaped object

that has a highly specular surface. An interesting application for the proposed method is seen in Fig. 11. The object is a metal bolt that has a hexagonal-shaped head. The painted surface of the head is Lambertian in reflection, whereas the threaded section of the bolt is specular. Surface orientations are measured only along the thin edges of the threads since

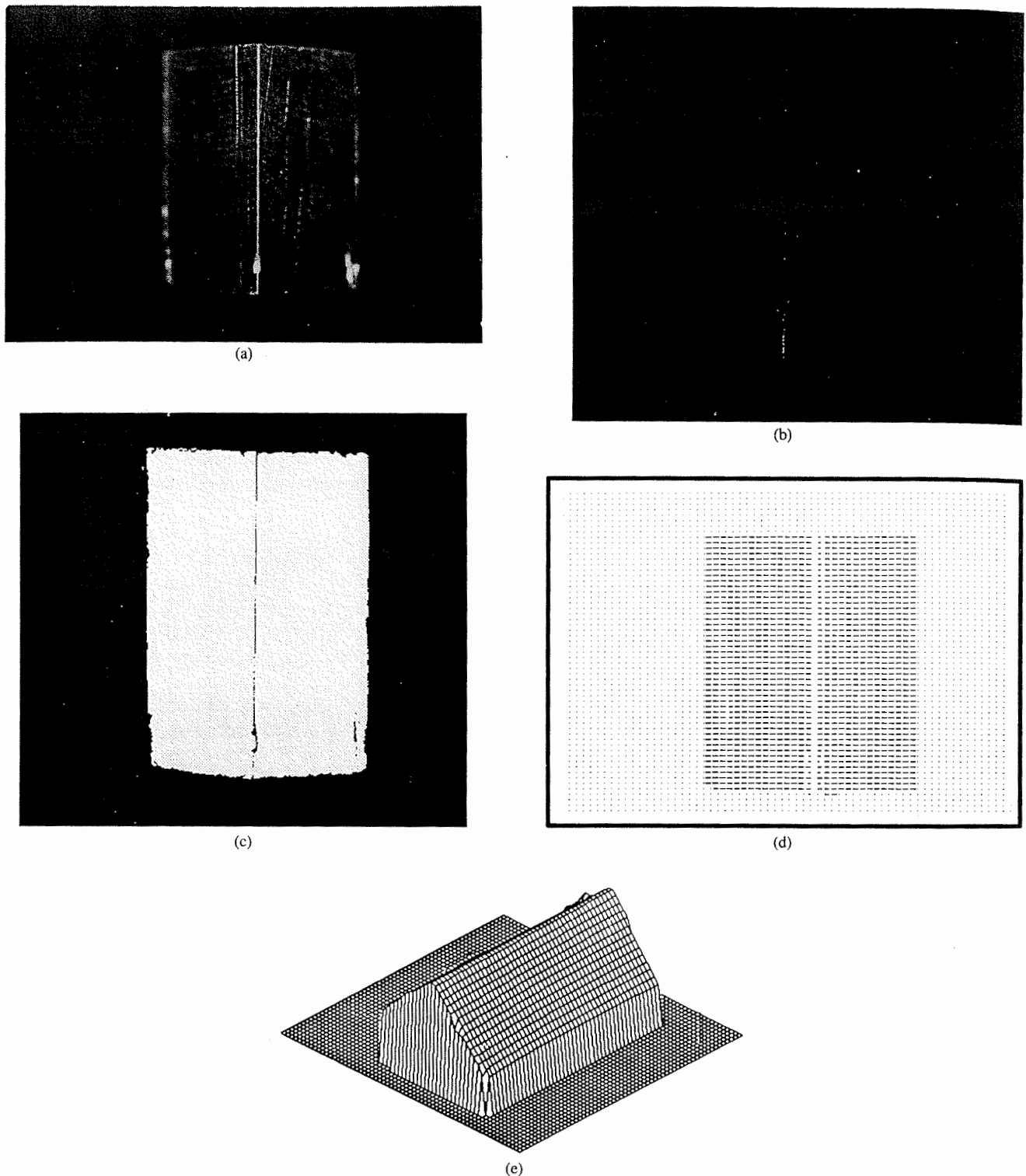


Fig. 10. Prism-shaped metallic object with a specular surface: (a) Object; (b) Lambertian strength; (c) specular strength; (d) needle map; (e) depth map.

surface orientations in the grooves between threads lie outside the range of orientations that the current two-dimensional system is capable of measuring. While generating needle maps, surface orientations are sampled to make room for the display of needles. In the process of sampling, a considerable number of orientations measured on the threads of the bolt are lost. Hence, the orientations measured on a few threads

are displayed at a higher resolution. We have not included a depth map of the bolt because its needle map has many disjoint regions and is difficult to integrate.

All the above experiments were conducted on surface points that are either Lambertian or specular. A major advantage of the photometric sampling method, over other shape extraction techniques, lies in its ability to determine the shape and

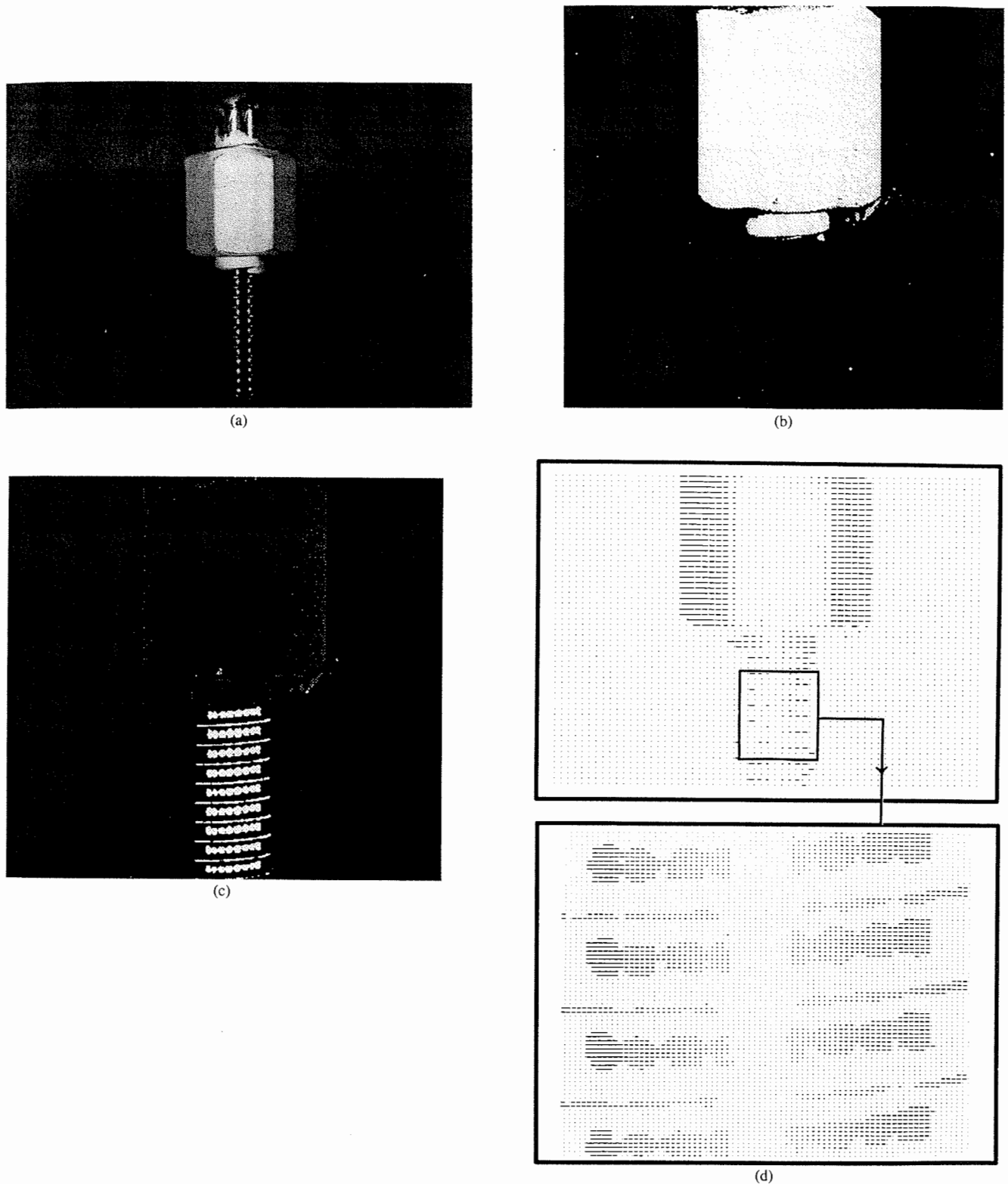


Fig. 11. Metal bolt. The head of the bolt is painted and has a Lambertian surface, whereas the threaded section has a specular surface: (a) Object; (b) Lambertian strength; (c) specular strength; (d) needle map.

reflectance of hybrid surfaces. The surfaces of many manufactured plastic objects seem to fall into this category. The Lambertian component is produced by the internal scattering mechanism, whereas the sharp specular component results from the smoothness of the surface. Fig. 12 shows the photo

of a plastic object that is cylindrical in shape. As expected, nonzero Lambertian and specular strengths are seen in the reflection images.

An important feature of all the above results is that the surface properties at a pixel are computed solely from the

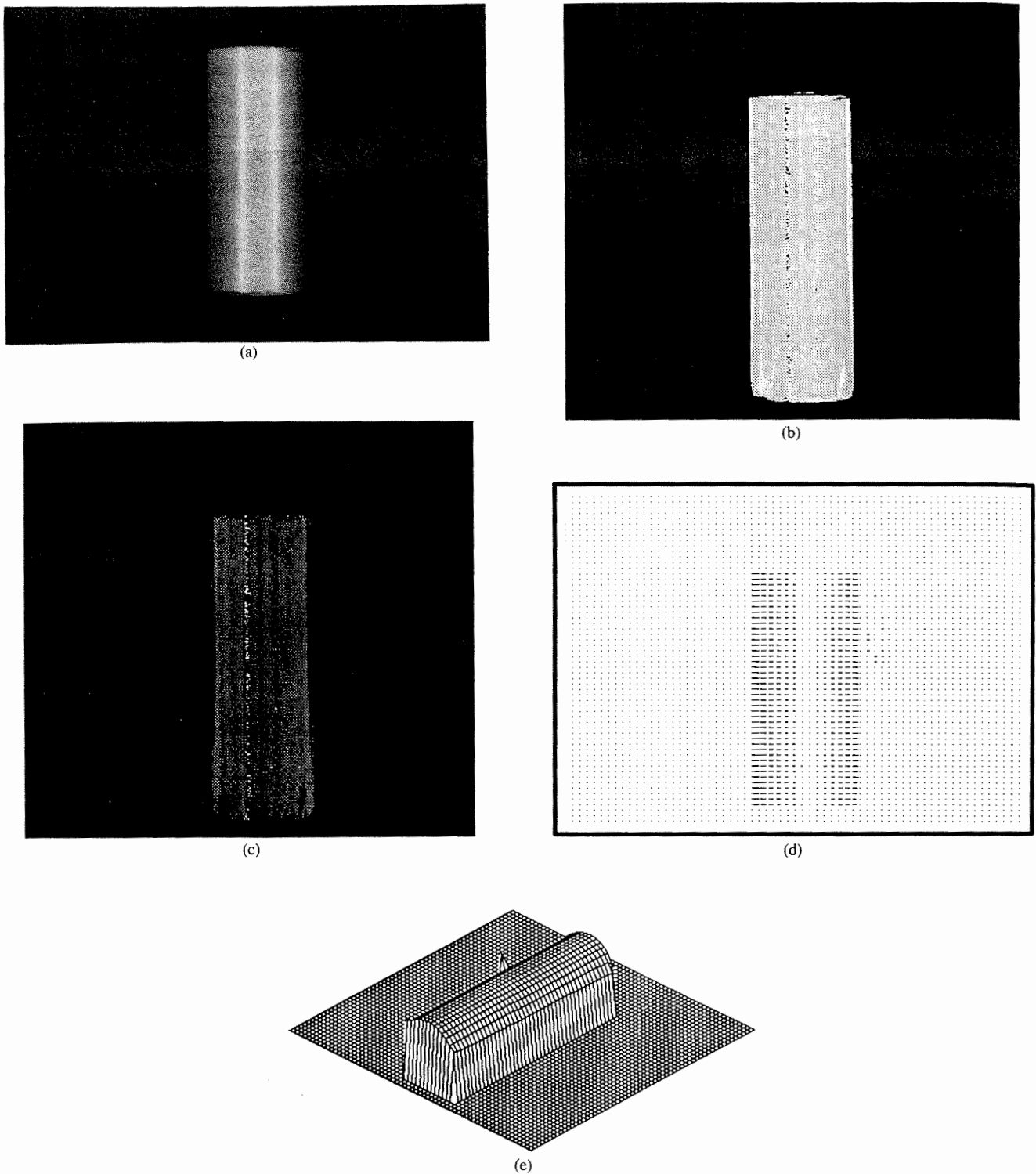


Fig. 12. Cylindrical plastic object with a hybrid surface: (a) Object; (b) Lambertian strength; (c) specular strength; (d) needle map; (e) depth map.

intensities recorded at that pixel. The needle maps and reflectance images have not been subjected to any filtering or regularization operations. An error analysis was conducted to estimate the measurement accuracy of the current setup. Fig. 13 shows the surface orientations measured along a horizontal section of the hybrid cylindrical sample shown in Fig. 12. The actual orientation values along the section are computed using

the known radius of the cylinder. The errors in the measured orientations  $\theta_{\text{error}}$  are plotted in Fig. 14. From these errors, the following quantities were computed: *mean orientation error* =  $1.022^\circ$ , *mean absolute orientation error* =  $1.656^\circ$ , *standard deviation in orientation error* =  $0.189^\circ$ , and *maximum orientation error* =  $5.596^\circ$ . The estimated reflectance parameters were found to be consistent with the appearance

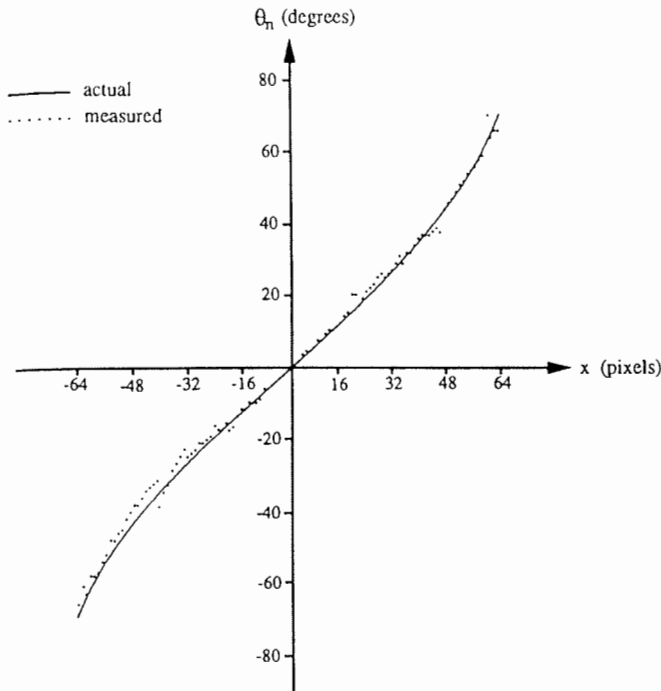


Fig. 13. Measured and actual surface orientations along a horizontal section of the hybrid cylindrical object shown in Fig. 12.

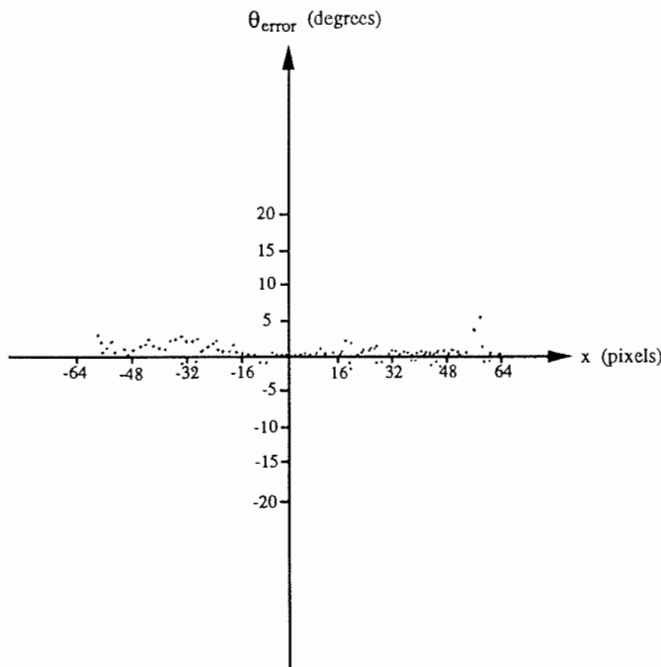


Fig. 14. Errors in measured orientations computed from the measured and actual orientation values plotted in Fig. 13.

of the surface samples used to conduct the above experiments. A more formal evaluation of the reflectance measurement accuracy of the proposed method is in progress.

VI. CONCLUSIONS

We conclude this paper with the following remarks:

- The hybrid reflection model is obtained by studying various reflection mechanisms and by making assumptions related to the microscopic structure of the surface.

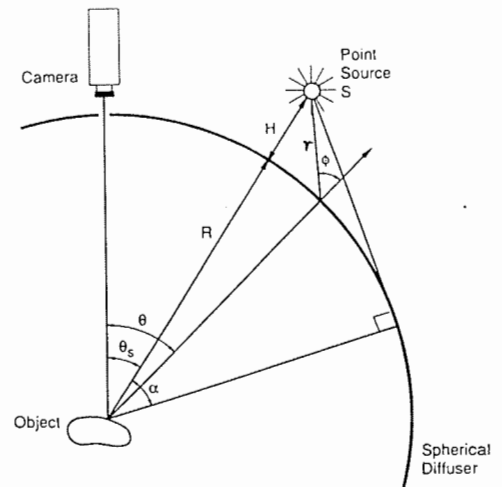


Fig. 15. Extended source.

- The photometric sampling method uses uniformly distributed source directions to obtain a set of image intensity values at each surface point.
- Surface illumination using extended light sources makes it possible to capture both Lambertian and specular reflections in the image intensities.
- The extraction algorithm uses the image intensities to simultaneously recover shape and reflectance parameters of hybrid surfaces, including Lambertian and specular surfaces. Objects comprised of combinations of the aforementioned surface classes can also be handled by the algorithm.
- The extraction algorithm is local in that the orientation and reflectance of a surface point are computed solely from image intensities recorded at that point.
- Accurate orientation estimates are obtained by using both Lambertian and specular components of the image intensities.

We are currently in the process of extending the theory and experimental setup to three dimensions. We are also interested in using the most general form of the reflectance model described in Section II in order to increase the range of surfaces that can be handled by the photometric sampling method.

APPENDIX A

GENERATING EXTENDED SOURCES

There are numerous ways of generating extended light sources. In this Appendix, we present the approach that we have chosen to use. An extended source can be generated by illuminating a sheet of light-diffusing material with a point light source. Fig. 15 illustrates the illumination of a section of a circular diffuser of radius  $R$ . The point source is placed at a distance  $H$  from the diffuser's surface, and the viewed object is placed at the center of the circle. Let us assume that the diffuser is "ideal," i.e., incident energy is scattered equally in all directions. Then, the radiance<sup>4</sup>  $L(\theta, \theta_s)$  of the

<sup>4</sup> Radiance is defined as the flux emitted per unit of foreshortened surface area per unit solid angle. Radiance is measured in watts per square meter per steradian ( $W \cdot m^{-2} \cdot sr^{-1}$ ).

inner surface of the diffuser is proportional to the irradiance<sup>5</sup>  $E(\theta, \theta_s)$  of the outer surface of the diffuser

$$L(\theta, \theta_s) = CE(\theta, \theta_s) \quad (20)$$

where  $C$  is a constant of proportionality. The analytic expression for the surface irradiance  $E(\theta, \theta_s)$  may be derived from the basics of radiometry as

$$E(\theta, \theta_s) = \frac{I \cos \phi}{r^2} \quad (21)$$

where  $I$  is the radiant intensity<sup>6</sup> of the point source  $S$ . The radiance of the extended source may be determined by expressing the variables  $r$  and  $\phi$  in (21) in terms of the parameters  $R$ ,  $H$ , and  $\theta_s$  of the illumination geometry:

$$L(\theta, \theta_s) = \frac{CI[(R+H) \cos(\theta - \theta_s) - R]}{[(R+H - R \cos(\theta - \theta_s))^2 + (R \sin(\theta - \theta_s))^2]^{3/2}} \quad (22)$$

Throughout this paper, the position of an extended source is denoted by the angle  $\theta_s$  of the point source used to generate the extended source. The radiance function  $L(\theta, \theta_s)$  is symmetric or even, with respect to the source direction ( $\theta = \theta_s$ ), and its magnitude decreases as  $\theta$  deviates from  $\theta_s$ . Points on the diffuser that lie in the interval  $\theta_s - \alpha < \theta < \theta_s + \alpha$  receive light from the point source  $S$ . Points that lie outside this interval are occluded from the point source by points that lie in the interval. Thus,  $L(\theta, \theta_s) = 0$  for  $\theta < \theta_s - \alpha$  and  $\theta > \theta_s + \alpha$ . The *source termination angle*  $\alpha$  is determined from Fig. 15 to be

$$\alpha = \cos^{-1} \frac{R}{R+H} \quad (23)$$

#### ACKNOWLEDGMENT

The authors are grateful to B. K. P. Horn, G. Klinker, and J. Krumm for their valuable comments. The members of the VASC center at Carnegie Mellon University provided many useful suggestions.

#### REFERENCES

- [1] P. Beckmann and A. Spizzichino, *The Scattering of Electromagnetic Waves from Rough Surfaces*. New York: Macmillan, 1963.
- [2] E. N. Coleman and R. Jain, "Obtaining 3-dimensional shape of textured and specular surface using four-source photometry," *Comput. Graphics Image Processing*, vol. 18, no. 4, pp. 309-328, Apr. 1982.
- [3] G. Healey and T. O. Binford, "Local shape from specularity," in *Proc. Image Understanding Workshop*, Feb. 1987, vol. 2, pp. 874-887.
- [4] B. K. P. Horn, "Shape from shading: A method for obtaining the shape of a smooth opaque object from one view," MIT Project MAC Internal Rep. TR-79 and MIT AI Lab. Tech. Rep. 232, Nov. 1970.
- [5] B. K. P. Horn, "Image intensity understanding," *Artificial Intell.*, vol. 8, no. 2, 1977.
- [6] K. Ikeuchi and B. K. P. Horn, "Numerical shape from shading and occluding boundaries," *Artificial Intell.*, vol. 17, nos. 1-3, pp. 141-184, Aug. 1981.
- [7] K. Ikeuchi, "Determining surface orientations of specular surfaces by using the photometric stereo method," *IEEE Trans. Patt. Anal. Mach. Intell.*, vol. PAMI-3, no. 6, pp. 661-669, Nov. 1981.

<sup>5</sup> Irradiance is defined as the incident flux density and is measured in watts per square meter ( $W \cdot m^{-2}$ ).

<sup>6</sup> Radiant intensity of a source is defined as the flux exiting per unit solid angle and is measured in watts per steradian ( $W \cdot sr^{-1}$ ).

- [8] P. Kubelka and F. Munk, "Ein Beitrag zur Optik der Farbanstriche," *Z. tech. Physik*, vol. 12, p. 593, 1931.
- [9] J. H. Lambert, *Photometria Sive de Mensura de Gratibus Luminis, Colorum et Umbrae*. Augsburg: Eberhard Klett, 1760.
- [10] S. K. Nayar, K. Ikeuchi, and T. Kanade, "Extracting shape and reflectance of Lambertian, specular, and hybrid surfaces," CMU-RI-TR-88-14, Aug. 1988.
- [11] S. K. Nayar, K. Ikeuchi, and T. Kanade, "Surface reflection: Physical and geometrical perspectives," CMU-RI-TR-89-7, Mar. 1989.
- [12] F. E. Nicodemus, J. C. Richmond, J. J. Hsia, I. W. Ginsberg, and T. Limperis, "Geometrical considerations and nomenclature for reflectance, NBS Monograph 160, Nat. Bureau Standards, Boulder, CO, Oct. 1977.
- [13] A. P. Pentland, "Local shading analysis," *IEEE Trans. Patt. Anal. Mach. Intell.*, vol. PAMI-6, no. 2, pp. 170-187, Mar. 1984.
- [14] J. Reichman, "Determination of absorption and scattering coefficients for nonhomogeneous media 1: Theory," *Appl. Optics*, vol. 12, no. 8, pp. 1811-1815, Aug. 1973.
- [15] A. C. Sanderson, L. E. Weiss, and S. K. Nayar, "Structured high-light inspection of specular surfaces," *IEEE Trans. Patt. Anal. Mach. Intell.*, vol. 10, no. 1, pp. 44-55, Jan. 1988.
- [16] W. M. Silver, "Determining shape and reflectance using multiple images," S. M. thesis, Dept. Elect. Eng. Comput. Sci., MIT, Cambridge, MA, June 1980.
- [17] K. Torrance and E. Sparrow, "Theory for off-specular reflection from roughened surfaces," *J. Optical Soc. Amer.*, no. 57, pp. 1105-1114, 1967.
- [18] R. J. Woodham, "Photometric stereo: A reflectance map technique for determining surface orientation from image intensity," *Proc. SPIE*, vol. 155, pp. 136-143, 1978.



**Shree K. Nayar** (M'90) received the B.S. degree in electrical engineering from the Birla Institute of Technology, Ranchi, India, in 1984 and the M.S. degree in electrical and computer engineering from the North Carolina State University, Raleigh, in 1986.

He is currently a Research Assistant at the Robotics Institute, Carnegie Mellon University, Pittsburgh, PA, and is working towards the Ph.D. degree in electrical and computer engineering.

Since 1988, he has been supported for his dissertation work by a Westinghouse research fellowship. In the summer of 1989, he was a Visiting Research Scientist at the Production Engineering Research Laboratory, Hitachi Ltd., Yokohama, Japan. He has been awarded several patents for his inventions related to machine vision. His research interests include machine vision, robotics, and artificial intelligence.



**Katsushi Ikeuchi** (M'89) is a senior research scientist (associate professor level) of computer science and robotics at Carnegie Mellon University, Pittsburgh, PA. He received B. Eng. degree in mechanical engineering from Kyoto University, Kyoto, Japan, in 1973, and the M. Eng. and Ph.D. degrees in information engineering from the University of Tokyo, Tokyo, Japan, in 1975 and 1978, respectively.

Since then, he has held several research positions at the Artificial Intelligence Laboratory, Massachusetts Institute of Technology, Cambridge, Electrotechnical Laboratory, Ministry of International Trade and Industry (Japanese government), and the School of Computer Science, Carnegie Mellon University. His research accomplishments in image understanding include the development of "smoothness constraints" wherein the neighboring points have the similar surface orientations, by which he recovered shape from shading and shape from texture, iteratively. He has also pioneered the use of specular reflections to recover surface orientations. Instead of discarding specular reflections, he actively used them for recovering shape and reflectance. Currently, he has been developing a vision algorithm compiler, which converts an object and sensor model into a vision program automatically.



**Takeo Kanade** (SM'88) is Professor of Computer Science and Robotics at Carnegie Mellon University, Pittsburgh, PA, and codirector of the Robotics Institute. He received the Ph.D. degree in information science from Kyoto University, Japan, in 1974.

After having taught at at Kyoto University at Associate Professor of Information Science, he joined Carnegie Mellon in 1980. He has worked on various problems involving vision, sensors, manipulators, and mobile robots. His best-known accomplishments include a theory of the Origami World

for shape recovery from line drawings, development of new direct-drive arm technologies (DD Arm I and DD Arm II), which were first conceived and prototyped at CMU, and development of a vision navigation system for the

Navlab (a van with onboard sensors and computers). He is currently engaged in three major robotics research programs at CMU as the Principal Investigator: Image Understanding, Natural Outdoor Navigation (NAVLAB) Vision System, and Planetary Exploration Robot.

Dr. Kanade has authored and edited three books and authored more than 80 papers and technical reports. He also serves the NASA Advanced Technology Advisory Committee (which is a congressionally mandated committee) as a consultant. He is the founding editor of *International Journal of Computer Vision*, and is an Administrative Committee member of IEEE Robotics and Automation Society. He served as a General Chairman of IEEE International Conference on Computer Vision and Pattern Recognition (1983) and a Vice Chairman of IEEE International Conference on Robotics and Automation (1986).

he,  
inis.  
I re-  
-TR-  
sical  
and  
re-  
CO,  
nal.  
ents  
no.  
igh-  
ch.  
im-  
ge,  
om  
14,  
for  
IE,  
  
ee  
of  
S.  
m  
in  
  
re  
y,  
),  
g-  
r-  
,  
h  
il  
s